TU Delft

Delft University of Technology

Two-Dimensional Reconstruction of Ionospheric Plasma Density Variations Using Swarm

Fæhn Follestad, A.; Clausen, L. B.N.; Miloch, W. J.; van den IJssel, J.; Haagmans, R.

DOI
10.1029/2019SW002406

Publication date
2020

Document Version
Final published version

Published in
Space Weather

Citation (APA)
Fæhn Follestad, A., Clausen, L. B. N., Miloch, W. J., van den IJssel, J., & Haagmans, R. (2020). Two-Dimensional Reconstruction of Ionospheric Plasma Density Variations Using Swarm. *Space Weather*, *18*(6), Article e2019SW002406. https://doi.org/10.1029/2019SW002406

Important note
To cite this publication, please use the final published version (if applicable).
Please check the document version above.

Copyright
Other than for strictly personal use, it is not permitted to download, forward or distribute the text or part of it, without the consent of the author(s) and/or copyright holder(s), unless the work is under an open content license such as Creative Commons.

Takedown policy
Please contact us and provide details if you believe this document breaches copyrights.
We will remove access to the work immediately and investigate your claim.

This work is downloaded from Delft University of Technology.
For technical reasons the number of authors shown on this cover page is limited to a maximum of 10.

Space Weather

RESEARCH ARTICLE
10.1029/2019SW002406

Two-Dimensional Reconstruction of Ionospheric Plasma Density Variations Using Swarm

A. Fæhn Follestad[1], L. B. N. Clausen[1], W. J. Miloch[1], J. van den IJssel[2], and R. Haagmans[3]

[1]Department of Physics, University of Oslo, Oslo, Norway, [2]Department of Space Engineering, Delft University of Technology, Delft, The Netherlands, [3]ESA/ESTEC, Noordwijk, The Netherlands

Key Points:
- We present a new method for reconstructing 2-D plasma density variations using GPS TEC from the Swarm satellites
- The results agree well with Langmuir probe density measurements and ground-based TEC observations
- The method allows for monitoring plasma density in the ionosphere using satellites in low Earth orbit

Supporting Information:
- Supporting Information S1

Correspondence to:
A. Fæhn Follestad,
a.k.f.follestad@fys.uio.no

Citation:
Fæhn Follestad, A., Clausen, L. B. N., Miloch, W. J., van den IJssel, J., & Haagmans, R. (2020). Two-dimensional reconstruction of ionospheric plasma density variations using Swarm. *Space Weather*, *18*, e2019SW002406. https://doi.org/10.1029/2019SW002406

Received 14 NOV 2019
Accepted 28 APR 2020
Accepted article online 19 MAY 2020

This article was prematurely published without the authors' corrections. Corrections were made on 27 June 2020, to incorporate the authors' changes.

©2020. The Authors.
This is an open access article under the terms of the Creative Commons Attribution-NonCommercial-NoDerivs License, which permits use and distribution in any medium, provided the original work is properly cited, the use is non-commercial and no modifications or adaptations are made.

Abstract Space weather phenomena such as scintillations of Global Navigation Satellite Systems (GNSS) signals are of increasing importance for aviation, the maritime, and civil engineering industries. The ionospheric plasma irregularities causing scintillations are associated with strong gradients in ionospheric plasma density. To provide nowcasts and forecasts of space weather effects, it is vital to monitor the ionosphere and detect strong density variations. To reconstruct plasma density variations in the polar cap ionosphere, we use total electron content (TEC) estimates from the Swarm satellites' GPS receivers. By considering events where the Swarm satellites are in close proximity, we obtain plasma density variations by inverting TEC measurements on a two-dimensional grid. We first demonstrate the method using synthetic test data, before applying it to real data. The method is validated using in situ Langmuir probe measurements and ground-based TEC observations. We find that the new method can reproduce density variations, although it is sensitive to the geometry of the Swarm satellite constellation and to the calculated plasma temperature. Our proposed method opens new possibilities for ionospheric plasma monitoring that uses GPS receivers aboard low Earth orbit (LEO) satellites.

1. Introduction

Space weather comprises a number of phenomena that affect the Earth's magnetosphere, thermosphere, and ionosphere. The effects of space weather on technology include power grid failure, disruptions of the electronic systems of satellites, or disturbances of radio communications and satellite-based positioning and navigation systems such as Global Navigation Satellite Systems (GNSS). Our society and industry are increasingly dependent on technology, and in particular on satellite based communication and navigation systems. Understanding and monitoring the conditions related to space weather effects on such systems are essential steps toward space weather forecasting.

Satellite signals propagating through the ionosphere can undergo disturbances that manifest as rapid fluctuations in phase and amplitude, called scintillations (Kintner et al., 2007; Yeh & Liu, 1982). Scintillations of transionospheric radio waves are associated with irregularities in electron density, which can result from different phenomena such as storm-enhanced ionospheric plasma density, auroral particle precipitation and/or polar cap patches (Alfonsi et al., 2011; De Franceschi et al., 2008; Jin, Moen, et al., 2014; Jin et al., 2015; Jin et al., 2016; Mitchell et al., 2005; Moen et al., 2013; Prikryl et al., 2010, 2015; Spogli et al., 2009). Scintillations degrade GNSS position accuracy and can cause loss of lock for the GNSS receiver (Aarons, 1982; Garner et al., 2011; Jacobsen & Andalsvik, 2016; Jin & Oksavik, 2018).

One source of GNSS scintillations in the polar regions are the steep density gradients found on the edges of polar cap patches (e.g., Buchau et al., 1985; Basu et al., 2002; Clausen et al., 2016; Jin, Moen, et al., 2014; Jin et al., 2016; Meeren et al., 2015; Prikryl et al., 2010; Spogli et al., 2009; Weber et al., 1986). These steep density gradients allow the Gradient Drift Instability (GDI) to develop, so that the plasma becomes structured and affects radio signals propagating throughout the ionosphere. Polar cap patches are usually defined as at least two times the density of the surrounding plasma (Crowley, 1996).

Observing and monitoring the polar cap ionosphere and detecting patches is a vital area of study for predicting space weather effects. This is traditionally done using ground-based radars, in situ satellites and rockets. Additionally, combining data from different sources allows for reconstructing plasma density in the ionosphere. One such method is the ionospheric tomography, a concept that have been developed significantly

over the past decades. Different solution algorithms for solving the linear set of equations have been developed, such as iterative techniques, multiplicative algebraic reconstruction technique (MART), and quadratic programming (Raymund et al., 1990; Raymund, 1995; Pryse et al., 1998). Present tomographic reconstruction techniques use input from ground-based GNSS or NNSS receivers (Chen et al., 2016; Leitinger et al., 1997; Spencer et al., 1998; Tsai et al., 2002; Zhou et al., 2015), often in combination with low Earth orbit (LEO) satellites (Li et al., 2012), NNSS satellites (Pryse & Kersley, 1992; Raymund et al., 1993), or ionosondes (Dos Santos Prol et al., 2019; Ma et al., 2005).

There have also been some successful attempts to create three dimensional, time-dependent ionospheric density reconstructions (Bust et al., 2004, 2007; Mitchell et al., 2005). The common feature for these methods is that they rely on ground-based observations of some kind.

The use of ground-based observations inherently restricts the coverage that the tomographic method can provide. Satellites, on the other hand, can provide global coverage for monitoring ionospheric plasma. Some work has been done in the past to detect polar cap patches using GPS receivers aboard satellites, which have used the total electron content (TEC) directly to define a patch. For example, Noja et al. (2013) used the CHAMP satellite to study the climatology of polar cap patches using the GPS receiver on board. In their study, patch is defined as a positive TEC slope followed by a negative slope within a 200 s sliding window (= 1,500 km arc). A similar approach was used by Coley and Heelis (1995), who used the Dynamics Explorer 2 satellite. Additionally, the in situ plasma density gradients from the Langmuir probes aboard the Swarm satellites have been used to detect polar cap patches and study polar cap patch climatology (see Goodwin et al., 2015; Spicher et al., 2017).

This paper presents a novel approach to reconstruct ionospheric density variations in the horizontal plane, using the Swarm satellites and their GPS receivers. Satellite based measurements open a possibility for monitoring the polar ionosphere over less accessible regions, such as oceans or Antarctica. The method is easily extendable to any LEO satellite with a dual-frequency GPS receiver (or other Global Navigation Satellite System receiver that can provide TEC estimates), promising better than ever coverage of the polar cap in terms of monitoring the ionosphere.

2. Instrumentation

The Swarm mission comprises three satellites launched by the European Space Agency (ESA) in 2013. The main goal of the Swarm mission is to study Earth's geomagnetic field variations with better-than-ever temporal and spatial resolutions. The three-satellite configuration enables creation and validation of global models with high accuracy, because the satellites provide measurements at three different locations simultaneously. For an in-depth review of the Swarm mission's objectives and technical details, see, for example, Friis-Christensen et al. (2006) and Olsen et al. (2013).

Swarm Satellites A and C orbit the Earth in tandem, at an initial altitude of 462 km and an inclination of 87.35°. Swarm B orbits at an altitude of approximately 511 km, at inclination 87.75°. The orbits were initially at approximately the same local time (pearls-on-a-string configuration). The local time separation between Swarm B and Swarm A/C increases with time.

2.1. Swarm GPS Receiver

The inversion technique described in this paper, uses data from the GPS receivers onboard Swarm as input. Each Swarm satellite is equipped with an eight-channel dual-frequency GPS receiver. For a detailed description of Swarm's GPS receivers, see, for example, van den IJssel et al. (2016). The dual-frequency feature allows the receiver to estimate the TEC, see, for example Jin, Cardellach, et al., (2014). The TEC is defined in equation (1), where n is the plasma density per m^3 and s is the spatial variable along the raypath. TEC is provided at 1 Hz from 15 July 2014 and onward (van den Ijssel et al., 2015).

$$TEC = \int_{s1}^{s2} n \, \mathrm{d}s \tag{1}$$

The integral limits ($s1$, $s2$) are the locations of the GPS receiver and the tracked GPS satellite. In this study, the GPS receiver is located on the Swarm satellite. Thus, in this study, TEC is a measure of the number of electrons in a cylinder with cross-sectional area 1 m^2 and length s between the two spacecrafts,

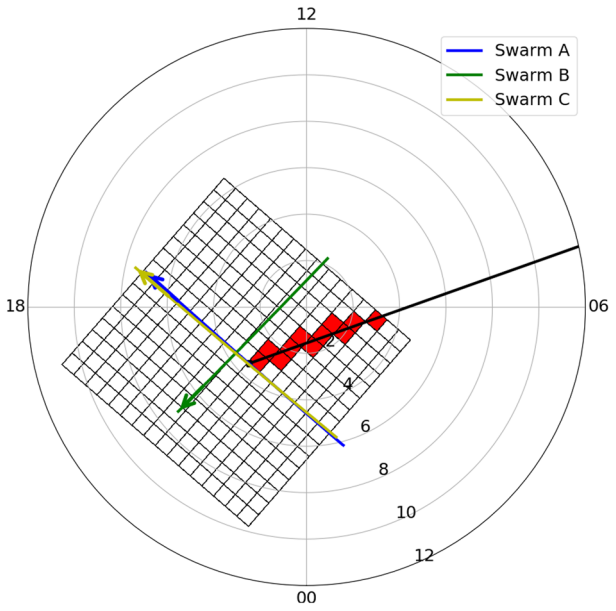

Figure 1. Grid used for inversion and Swarm trajectories corresponding to 29 November 2017, 15:04–15:06:50. Swarm A is blue, Swarm B is green, and Swarm C is yellow. The black line indicates direction to a GPS satellite tracked by Swarm A at time t, and the cells with plasma density contribution to TEC measured at Swarm A at time t are colored red. The coordinate system is Magnetic Local Time (MLT) with noon to the top of the figure versus magnetic latitude (MLAT).

that is, the GPS satellite and the Swarm satellite. The measurement is given in terms of TEC units, where 1 TECu = 10^{16} el m^{-2}.

2.2. Swarm Langmuir Probe

We also include data from the Langmuir probes from the Electric Field Instrument onboard Swarm. Each Swarm satellite carries two Langmuir probes, as part of the Electric Field Instrument at the front of the satellite. The Langmuir probes aboard Swarm estimate electron density from current measurements at a predefined probe potential (Knudsen et al., 2017). The electron density is provided in units of m^{-3} and is sampled at 2 Hz (Jin et al., 2019; Knudsen et al., 2017).

2.3. Ground-Based GPS Receiver Network

To validate our results, we use the ground-based world wide GPS receiver network obtained from the Madrigal CEDAR Database (Rideout & Coster, 2006), which provide estimated global TEC maps. The data are processed using the minimum scallop technique, presented in detail by Rideout and Coster (2006) and Vierinen et al. (2016). In the polar cap, the TEC is calculated at 5 min intervals, binned in 1° latitude and 1° longitude. We apply median filtering, a technique that eliminates noise and smoothes data by taking the median over a moving boxcar window for each bin, where the window size is 3 × 3 bins (Thomas et al., 2013).

3. Methodology

Our reconstruction technique estimates density variations in the ionosphere using observations from Swarm's GPS receivers. The technique is based on the fact that if waves, such as GPS signals, traverse the same volume of space in several different directions, some property of the traversed volume can be reconstructed using observations by the different waves/signals of said property. Applied to our investigation, we will use the integrated quantity of TEC, measured along various paths through a volume surrounding each satellite, to reconstruct local plasma density variations by inversion in two dimensions.

In particular, we will focus on events when the lower satellite pair (Swarm A and C) and the upper satellite (Swarm B) are in close proximity to each other. In such cases the number of rays (i.e., paths to GPS satellites along which TEC is measured) penetrating the volume around the satellites is maximized.

3.1. Reconstruction Algorithm Principle

The general principle behind the inversion algorithm is to assume that the measured TEC value along the Swarm-to-GPS satellite beam is the sum of contributions due to plasma density within each cell of a two-dimensional grid.

To present the concept, we choose an event were the satellite trajectories are nearly orthogonal. Additionally, we look for cases where the distance between the satellites is relatively small that is, less than 100 km. Based on the geometry of the crossing of the Swarm satellite orbits we establish a 2-D grid around the crossing point on 29 November 2017 between 15:04 and 15:06:50 UT, see Figure 1. The coordinate system is magnetic latitude (MLAT), where 0° is the magnetic north pole versus magnetic local time (MLT), and where 12 noon is toward the top of the page. The trajectories of Swarm A (blue), B (green), and C (yellow) are included. The black ray indicates a GPS satellite tracked by Swarm A at 108° azimuth at 15:05:20 UT. We sample Swarm GPS data every 10 s, and the number of cells in the grid (N) and the number of time steps (L) follows according to the duration of the selected event. We assume that the plasma density distribution is stationary during the time of the crossing, which is reasonable for short time intervals. In our case, the event has a duration of 170 s. If the interplanetary magnetic field (IMF) B_z component is negative, we expect ionospheric plasma density to convect with velocities of ≈500 m/s (Hosokawa et al., 2006; Weber et al., 1984). This velocity corresponds to 85 km during a 170 s interval, which is slightly more than the length of one grid cell, which is 71 km assuming a time step of 10 s and Swarm velocity 7.1 km/s.

At each time step during the crossing of the three satellites, the Swarm-to-GPS ray is traced through the grid to establish which grid cell (to be more precise, the plasma density within which grid cell) contributed to the measured TEC value. For example, at time step t, the value $TEC_{A-PRN_p}(t)$ quantifies the TEC between Swarm A and GPS satellite PRN_p at that time step. The situation is illustrated in Figure 1, where the TEC value measured at Swarm A at time t = 15:05:20 UT was due to the plasma densities in the 11 grid cells marked with red color, or expressed mathematically:

$$TEC_{A-PRN_p}(t) = \sum_{k=1}^{N} f_{ij(k)} n_{ij(k)} \tag{2}$$

where n is the plasma density, $ij(k)$ gives the row (i) and column (j) index of the kth bin from the grid that contributed. N is the total number of cells within the grid. The weighting factor $f_{ij(k)}$ represents a combination of different factors that affect the contribution of plasma density within a particular cell to a particular TEC measurement and will be discussed in the next sections.

By following all three Swarm S (S = A, B, C) satellites along their paths through the grid and accounting for all p tracked GPS satellites PRN_p ($p = 1, \ldots, 8$, the Swarm GPS receivers can track up to eight GPS satellites simultaneously) at all sampled times t_q ($q = 1, \ldots, Q$), during this interval, we can construct equations for TEC (equation (2)) and finally write them in the following matrix form:

$$TEC_{S-PRN_p}(t_q) = F_{S-PRN_p}(t_q) n_{ij(S-PRN_p)} \tag{3}$$

Equation (3) thus indicates the contributions to the measured TEC value $TEC_{S-PRN_p}(t_q)$, which is TEC measured by Swarm S tracking GPS satellite PRN_p at time t_q due to the plasma density at grid cell $ij(S-PRN_p, t_q)$, where i and j are grid cell indices. Note that the plasma density in each grid cell is assumed to be constant during the crossing; that is, there is no time dependence of the plasma density. The **TEC** matrix will have dimension $n_{row} \times 1$, where n_{row} is the total number of TEC measurements. For example, if all three Swarm satellites are used, and each of them tracks eight satellites at each of the Q time steps across the grid, $n_{row} = 3 \times 8 \times Q$. The density matrix **n** will have dimensions $n_{cell} \times 1$, where n_{cell} is the number of cells in the grid. Lastly, the **F** matrix will have dimension $n_{row} \times n_{cell}$.

The entries in the matrix **F** reflect the weight contribution of each grid cell, and it is a value between 0 and 1, depending on the weighting factors which will be explained later. Mathematically, the problem of solving for the plasma densities n reduces to a minimization problem on the 2-D grid, which will be described in more detail in section 3.3.

3.2. Improvement of Algorithm by Weighting

The weight matrix **F** describes the contribution from each grid cell to a particular raypath. In Figure 1, the cells with contribution were colored red. There was no distinction between the relative contribution from each of the red colored cells, although it is obvious that some of the grid cells will have a larger contribution to the TEC value than others. We want to capture the relative contributions from the different grid cells. We have therefore introduced several weightings that contribute to the value of **F**, which will be explained in detail in the subsequent paragraphs.

3.2.1. Weighting by Length

Considering Figure 1, we notice that the black ray that indicates GPS satellite direction passes diagonally through some cells, while it barely touches other cells. It is obvious that these cells will not contribute equally to TEC. We therefore introduce a length-dependent weighting factor:

$$ds_{ij(k)} = \frac{L_{ij(k)}}{L\sqrt{2}} \tag{4}$$

where $L_{ij(k)}$ is the length of the GPS signal path within the k cell given by the index $ij(k)$ and L is the side length of the grid cell; L is constant across the grid. If the Swarm-to-GPS ray passes exactly through the diagonal, the weighting factor $ds_{ij(k)} = 1$.

We note that discretization of the grid allows also for other weighting approaches. Another approach would be assigning thickness L to a discretized ray r_l, and determining the weight through the overlap of the grid cell area and the ray element area, such that

$$ds_{ij,(k)} = \frac{1}{A}\sum_{l=0}^{l_{max}} b_{ij(k),l} \tag{5}$$

where $A = L^2$ is the area of the grid cell and $b_{ij(k),l}$ is the common area of the ray element r_l and the grid cell at $ij(k)$; l_{max} is the total number of discretized ray elements considered within the grid cell. In case of rays parallel to the cell and traveling through the cell center, $ds_{ij(k)} = 1$. However, implementing such an algorithm is involved and computationally demanding, and for the sake of testing and demonstration of the method, we choose in this work the more straightforward weighting given in equation (4).

3.2.2. Weighting by Scale Height

Ionospheric particle density decreases with altitude, and the plasma density distribution along the Swarm-GPS ray needs to reflect this behavior. When two rays cross the same grid cell, but at different altitudes (e.g., due to different elevation angles), their contribution must be weighted accordingly. Another way of expressing this weighting is to say that the plasma densities that contribute to the line integral that is TEC are scaled to the satellite altitude. We therefore assume that the particle density decays exponentially with altitude (Kelley, 2009) and introduce a second weighting to account for the decrease in plasma density along the raypath:

$$a_{ij(k)} = \exp\left\{\frac{-h_{ij(k)}}{H}\right\} \tag{6}$$

where $h_{ij(k)}$ is the ray altitude above the satellite orbital altitude within cell $ij(k)$ based on the elevation angle and H is the ionospheric scale height:

$$H = \frac{k_B T}{\bar{m} g_h} \tag{7}$$

where k_B is Boltzmann's constant, T is the plasma temperature, $\bar{m}$ is the atomic mass and g_h is the altitude dependent gravitational constant. For $\bar{m}$, we assume that the F region plasma mainly consists of atomic oxygen (Kelley, 2009). The temperature is calculated based on comparing Langmuir probe density variations between two Swarm satellites and will be explained in section 3.2.3. This weighting factor ensures the exponential decay of density along the ray, so that grid cells where GPS-Swarm rays pass through with low altitude contribute more than those grid cells where the rays pass through at a high altitude. The scale height weighting factor also takes into account the different elevations of tracked GPS satellites.

3.2.3. Weighting by Plasma Temperature

We calculate the plasma temperature based on Langmuir probe density measurements. We assume that the ionospheric plasma density exhibits exponential decay, so that the density n_S at Swarm S altitude h_S can be described as follows:

$$n_S = n_0 exp\left\{\frac{-(h_S - h_0)}{H}\right\} \tag{8}$$

where n_0 is the plasma density at the peak density altitude h_0. We do not know n_0 and h_0. The solution is to consider the relative density between two Swarm satellites:

$$\frac{n_A}{n_B} = \frac{n_0 exp\left\{\frac{-(h_A - h_0)}{H}\right\}}{n_0 exp\left\{\frac{-(h_B - h_0)}{H}\right\}} = exp\left\{\frac{h_B - h_A}{H}\right\} \tag{9}$$

The plasma temperature is estimated by calculating the scale height by solving for H in equation 9, which allows us to take into account the altitude difference of Swarm A and B. Knowing the scale height H, we can easily find the plasma temperature from equation 7. In our calculations, we select a time window with length 20 s centered around the instant of closest approach between the satellite trajectories. We take the median temperature over the 20 s window as the plasma temperature for that crossing. As before, we assume that the plasma consists of atomic oxygen only.

An alternative to the approach described above is to use Swarms electric field instrument's thermal ion imager, which estimates plasma temperature from ion drift velocities. However, at present day, the data availability is not sufficient for our purpose.

3.2.4. Weighting by Height Difference Swarm A/C and B

Swarm A and C have an orbit altitude of about 462 km and Swarm B orbits at about 511 km, that is, 49 km above the other two. For the synthetic test case, we assume a plasma temperature of 1000 K, which gives a scale height of 57 km. Without knowing the peak plasma density or its altitude we can calculate the relative density level between Swarm A (or C) and B altitudes using equation 9. To calculate the height difference factor $\frac{n_B}{n_A}$, we use Langmuir probe density measurements averaged over a 20 s window. To account for the height difference, we multiply the contributions from Swarm B in each grid cell by $\frac{n_B}{n_A}$. The individual entries of the weight matrix **F** are then the product of the three weights described above.

3.3. Reconstruction of Ionospheric Plasma Density

When setting up the system of equations (equation 3), we have introduced some additional measures that improve the accuracy of the method. First, we remove a bias from the TEC estimates by subtracting the minimum value from each time series. Subtracting the background density is necessary because the GPS satellites are tracked at different azimuths and elevations, and the density between each Swarm and tracked satellite will vary significantly beyond the extent of the 2-D grid. The Swarm GPS receivers track GPS satellites at elevation angles ranging from a few degrees to almost 90° elevation. To eliminate multipath effects, we use a cutoff angle of 20°; that is, we only use GPS receiver data with elevation angle of 20° or higher for TEC observations.

As previously mentioned, to find the density in the grid shown in Figure 1, we must solve equation 3. The weight matrix **F** will generally not be invertible, hence we must solve the equation set by some other method. Here, we choose the gradient decent method, which is an iterative solution technique that reformulates the problem into a minimization exercise. The solution of equation 3 can be found by minimizing the linear least squares, which in our case can be expressed as follows:

$$\left\| \mathbf{F}_{S-PRN_p}(t_q) n_{ij(S-PRN_p)} - TEC_{S-PRN_p}(t_q) \right\|^2 \tag{10}$$

The principle of the method is to (Step 1) choose an initial guess for the minimum ($\mathbf{n}_0$) and calculate the gradient of equation 10, which gives us the descent direction for the next iteration (Step 2). We calculate the optimal step size (Step 3) using the golden section method (which we choose due to its computational efficiency), before calculating the new least square error (Step 4). We repeat Steps 2 through 4 until the solution converges within a given accuracy. A more detailed explanation of the gradient descent and golden section methods can be found in, for example, Snyman (2005).

4. Results

4.1. Synthetic Plasma Density Distribution

To test the quality of the inversion output from the method described in section 3, we use a test case with synthetic density distribution. We used the geometry of a real-world crossing of the three Swarm satellites, which occurred on 29 November 2017, at 15:04–15:06:50 UT. During the event, the Swarm satellites are situated in the Northern hemisphere. The resulting grid is shown in Figure 1. We created a synthetic plasma density distribution, where we assume a localized twofold plasma density enhancement. From the given plasma density distribution, we are able to create synthetic TEC time series for the three Swarm satellites.

Figure 2 shows the plasma density distribution on the grid corresponding to event on 29 November 2017, 15:04–15:06:50 UT. Panel (a) (left-hand side) shows the background density of 1 (normalized units), and a region of enhanced density near the point of closest approach between the Swarm satellites where the density is 2, that is, twice the background. The color bar on the right-hand side of Figure 2 is valid for both panels.

We assume that the Swarm satellites track GPS satellites at synthetic azimuth and elevation angles. In the next section we put certain constraints on the synthetic TEC time series to study the sensitivity of the inversion technique to certain parameters; but as a baseline we assume that each Swarm satellite observes 10 GPS satellites, evenly distributed between 20° and 40° elevation and 0–360° azimuth. Note that the only real data we use in this case are the Swarm trajectories, and the GPS receiver can in reality only track eight GPS

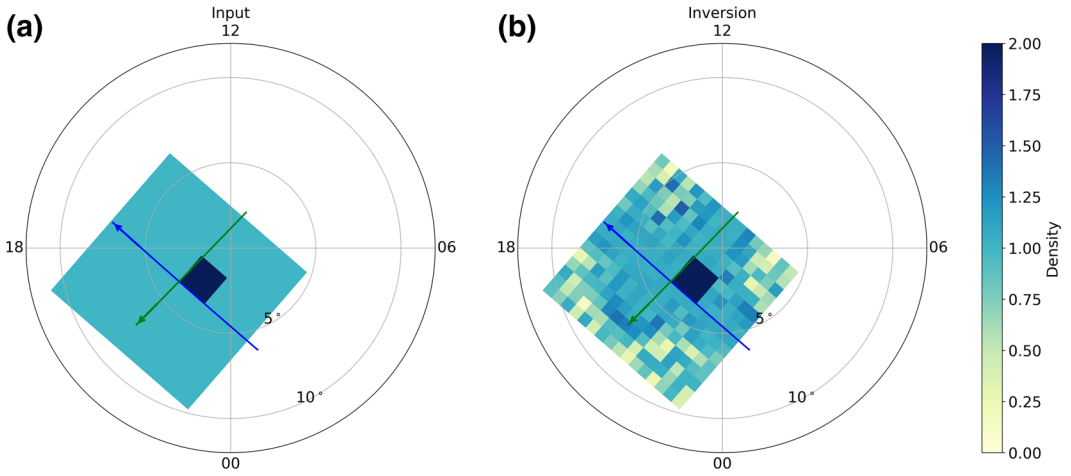

Figure 2. Grid and Swarm trajectories corresponding to 29 November 2017, 15:04–15:06:50, with synthetic background density and a block density enhancement in the center (a). The inversion results are shown in panel b. The color bar on the right-hand side applies to both panels.

satellites. Synthetic TEC time series are constructed by accumulating the weights from each grid cell along the beam multiplied by the input density given in that cell. The result of the reconstruction procedure is shown in Figure 2b. The two-dimensional enhancement in density has been reconstructed to a significant degree. The plasma density enhancement is calculated to be approximately 2, while the background density is around 1–1.3. That is, the background density is somewhat over predicted in the vicinity of the Swarm trajectories. Furthermore, the results are noisy and seem to under predict densities in the corners of the grid. Comparing the input and result, we obtain a root-mean-square (RMS) error of 0.263.

4.2. Grid Size and Edge Effects

There is a natural limitation to the possible grid size for the inversion, which is given by the Swarm trajectory geometry and the elevation of the tracked satellites. Numerically, it is the scale height weight factor that quantifies the limitation of the spatial extent of the grid. Assuming a minimum $a_{ij(k)}$ of 0.01 and plasma temperature $T = 1000$ K, we rearrange equation 6 to calculate an elevation dependent range. We find that if the elevation of the GPS satellite is 20°, the maximum distance from the Swarm trajectory to the outermost border of the farthest grid cell is 685 km. Likewise for a 40° elevation GPS satellite, the reach is 380 km.

Thus, the spatial limit of the grid size is highly dependent on the elevation of the tracked GPS satellites. To gain more insight and eventually set a size limit on the grid, we test the sensitivity of the method to grid size by moving the intensity enhancement in our test case away from the trajectory crossing point. Like in the previous section, we use elevations evenly distributed between 20° and 40° for the 10 tracked GPS satellites. The results of this exercise are presented in Figures 1– 3 in the supporting information. We find that a maximum distance from Swarm trajectory to the outer grid border of 580 km is a reasonable choice. Although some accuracy is lost around the edges, where the general tendency is that the density is underestimated, results are significant and reliable.

4.3. Sensitivity to Input Parameters

We have carried out sensitivity studies on several input variables that affect the results of the inversion procedure. We have run the analysis on the synthetic case outlined above and compared the different outcomes. This ensures that we use the optimal parameters when applying the inversion algorithm to real Swarm data. Detailed results from the analyses with plots of the reconstructed plasma density can be found in Figures S1–S17 in the supporting information. A summary of our findings is presented in Table 1.

The inversion procedure is more accurate when we have data from many GPS satellites and when the satellites are distributed around the entire 0–360° azimuth. Low GPS satellite elevation angle gives better accuracy, as well as larger grid size due to the scale height factor as discussed in sections 3.2.2 and 4.2. Analysis of several time step lengths showed that $t = 10$ s is a reasonable choice. A shorter time step should intuitively yield higher accuracy. However, we found that with time step $t = 5$ s, not only is the RMS higher

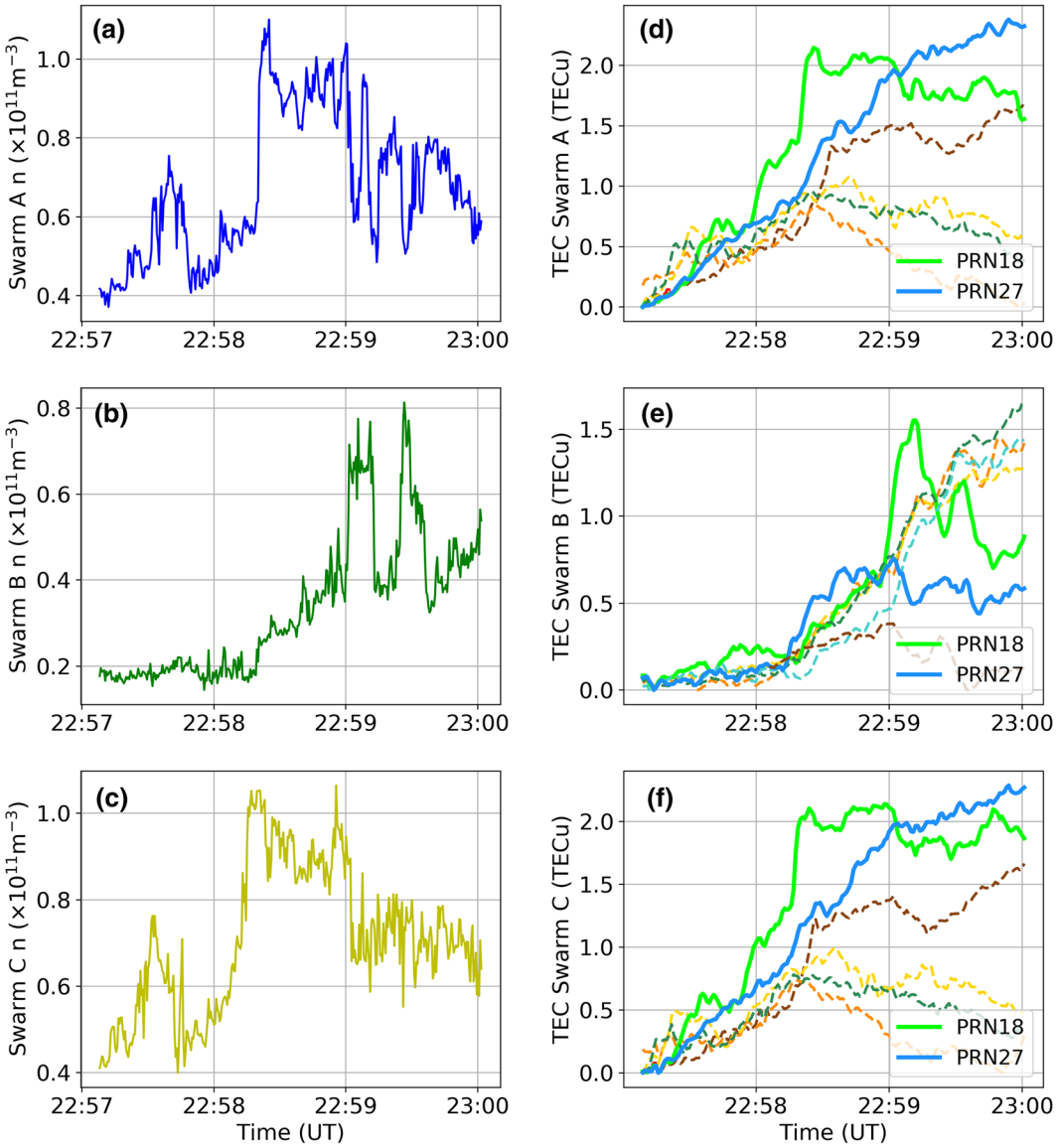

Figure 3. Results from 19 March 2017, from 22:57:08 to 23:00:02 UT. (a–c) The Langmuir probe plasma density measurements for Swarm A, B, and C. (d–f) The TEC calculations for different PRN for the three satellites, where the background TEC has been removed as described in section 3.3. For better readability, the legend is not shown, but the color coding for each PRN is consistent between the three panels, such that, for example, the green line refer to the same PRN throughout panels d–f. Two PRNs are highlighted with a solid line, see text for details.

than the baseline case (0.270), but the residual of the norm (that we are trying to minimize, see section 3.3) is higher than the baseline.

The plasma temperature will be calculated using Langmuir probe data for the real-world cases and is not an input parameter as such, but it is included in the sensitivity study to show that it has a significant effect on the precision of the inversion algorithm. For the synthetic case, we set the input plasma temperature to 1000 K, which gives an RMS error of 0.263. If we perform the inversion procedure with an plasma temperature of 3000 K, the RMS increases to 0.405, which is a significantly worse performance. This result highlights the importance of calculating the correct plasma temperature.

Additionally, we have run the synthetic case with only Swarm A and B contributing. This gave somewhat poorer results compared to the baseline. We conclude that two satellites can be used, but three satellites are preferred for better performance. Lastly, we tested the inversion procedure with a more complex density variation. We used one patch identical to the one shown in Figure 2, and added a second patch diagonally across

Table 1
Summary of Synthetic Case Sensitivity Analyses

	Input	RMS error
1	Baseline (see caption)	0.2625
2	No. of PRN: 1	0.5478
3	PRN azimuth: 0–180°	0.3970
4	PRN azimuth: 160–200°	0.4989
5	PRN elevation: All 20°	0.2263
6	PRN elevation: All 40°	0.3290
7	Time step length: 5 s	0.2703
8	Time step length: 20 s	0.3739
9	Plasma temperature: 2000 K	0.3039
10	Plasma temperature: 3000 K	0.4051
11	Swarm satellites: A, B	0.2796
12	Patch shape: Odd	0.2610

Note. The baseline input variables are the same as in section 4.1, and are as follows: 10 PRNs with azimuth 0–360° and elevations 20–40°, time step length 10 s, plasma temperature 1000 K, all three Swarm satellites are used and the patch is a square shape as shown in, for example, Figure 2. We ran sensitivity analysis where we changed one parameter at a time, while keeping the remaining input equal to the baseline. In total, we ran 1 baseline case and 11 sensitivity analyses.

the Swarm trajectory crossing point, at approximately 5° colatitude, 19–20 MLT. This two-patch density structure gave approximately the same result as the baseline synthetic case, with an RMS of 0.261.

4.4. Validation of Reconstruction Algorithm

In the previous section we presented a method to reconstruct plasma density variations in the ionosphere surrounding the Swarm satellites using synthetic data. We now apply the method to real-world data and compare our results to observations from ground-based GPS TEC measurements were such are available. The plasma temperature is calculated as described in section 3.2.3.

We search through the lifespan of the Swarm mission for cases where we can apply our inversion technique. To find suitable events, we have used the following restrictions:

- Maximum distance between Swarm A/C and B: 580 km
- Events located in the northern polar cap (MLAT > 70°)
- Event duration at least 90 s

This search gives yields about 520 cases. We run the reconstruction algorithm for each case. The following paragraphs show a few selected results.

4.4.1. Case 1: 19 March 2017

Case 1 is from 19 March 2017, from 22:57:08 to 23:00:02 UT. Swarm instrument data are shown in Figure 3. The left-hand side panels show Langmuir probe plasma density measurements for Swarm A (panel a), B (Panel b), and C (Panel c). The Langmuir probe density measurements in panel C show that Swarm A and C traverse a low-density region between 22:57 and 22:58 UT, where the density is approximately $n = 0.5 \times 10^{11}$ m^{-3}. At 22:58:15, Swarm C encounters a sharp increase in density, where the density doubles. Swarm A, in tandem with Swarm C, encounters a similar density intensification at the same time. The measured density slowly decreases toward the end of the event. Thus from Swarm A and C Langmuir probe data, we expect a density enhancement that lasts from the location corresponding to 22:58:15 UT to the end of the event. Swarm B travels almost perpendicularly to the lower satellite pair, and measures low densities ($n = 0.2 \times 10^{11}$ m^{-3} at the beginning of the event). The density measured by Swarm B's Langmuir probe increases around 22:59, although not as rapidly nor as severely as observed by the other two satellites. The peak in density of $n \approx 0.8 \times 10^{11}$ m^{-3} persists for about 30 s before the density decreases toward the end of the interval. From Swarm B Langmuir probe data, we expect a density increase at the location corresponding to a time interval approximately 22:59:00–22:59:30 UT.

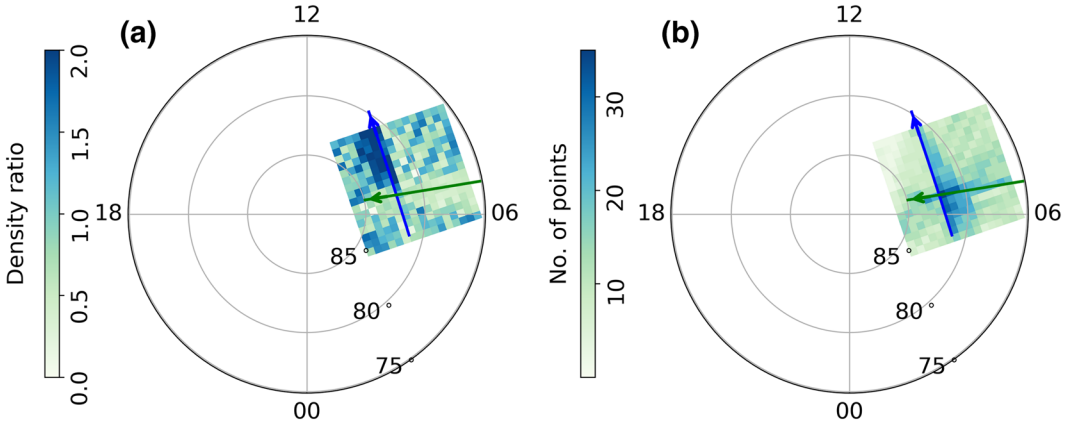

Figure 4. Results from 19 March 2017, from 22:57:08 to 23:00:02 UT. Panel (a) shows the density ratio (i.e., density in a grid cell density divided by the total average density across the grid) obtained with the inversion algorithm. The coordinate system is MLT-MLAT as in the previous figures, with Swarm A (blue) and Swarm B (green) trajectories overlaid. Panel (b) shows the number of data points within each grid cell, in the same coordinate system and overlaid Swarm trajectories as in panel (a).

The right-hand side plots in Figure 3 show TEC calculations for different GPS satellites for Swarm A/B/C in panels (d)–(f), respectively, with the background TEC removed separately for each PRN. For better readability, TEC measurements from two GPS satellites that will be discussed in detail are highlighted with solid lines. The legend is also shown for these two satellites. Note that the color coding for each GPS satellite is consistent between the three panels, such that for example the green line refers to the same GPS satellite throughout panels (d)–(f). Note also that for the Swarm satellites, 0° azimuth is the ram direction, starboard side is 90° azimuth, 180° azimuth is the aft, and port side is 270° azimuth.

During the event, GPS satellite PRN18 is tracked by Swarm A and C at ≈150° azimuth, that is, on the starboard/aft side of the satellite. PRN18's elevation is ≈40° throughout the event. TEC variations for PRN18 are shown in panels (d)–(f) in light green color. For Swarm A, TEC starts at about 0 TECu at the beginning of the event, before a significant increase to about 2.1 TECu around 22:58:15 UT. After that, the TEC level remains more or less constant throughout the event for PRN18 as observed by Swarm A. The results from Swarm C for PRN18 is similar to that of Swarm A, with a peak of about 2.1 TECu at 22:58:15. This TEC observation indicates that there is a density enhancement on the starboard side of the Swarm A/C pair. Swarm B's trajectory is nearly orthogonal to that of Swarm A/C, and tracks PRN18 at ≈225° azimuth, that is, port side/aft. TEC calculations start at 0 TECu in the beginning of the event, before a slight increase occurs at 22:59 UT, with a peak of 1.5 TECu. In the subsequent minutes, TEC declines to 0.9 TECu at the end of the event.

Swarm A and C track PRN27 at about 225° azimuth and 33° elevation, that is, to the port side/aft of the spacecraft. In panels (d) and (f), we observe that the TEC estimates show a steady increase throughout the event, starting at 0 TECu and ending at ≈2.4 TECu. We therefore expect a density enhancement on the port/aft side of Swarm A and C trajectories, that increases throughout the event. Swarm B tracks PRN27 at 280°, to the port side. Swarm B TEC shows a small increase from 3.1 to 3.8 occurring around 22:58:20 UT. We therefore anticipate a density increase along the Swarm A/C trajectory, and a small peak along Swarm B's trajectory occurring around 22:59 UT.

Results from our reconstruction algorithm are shown in Figure 4. Panel (a) shows the inversion in the MLT-MLAT coordinate system as in the previous figures, with Swarm A (blue) and Swarm B (green) trajectories overlaid. The density ratio (grid cell density divided by the average density across the grid) as a result of the inversion procedure in Panel (a) shows a density increase of about 3 times the background density located around 7–10 MLT, between 81° and 86° MLAT. The density enhancement is concentrated around the Swarm trajectory. Panel (b) shows the number of non-zero entries in **F** matrix for each grid cell. We note that there are relatively few data points in the patch region, implying that the real density is even higher.

Ground-based TEC observations are available for this date, but the coverage is patchy. The ground-based TEC measurements (not shown) indicate that there is a density enhancement starting at around 7 MLT,

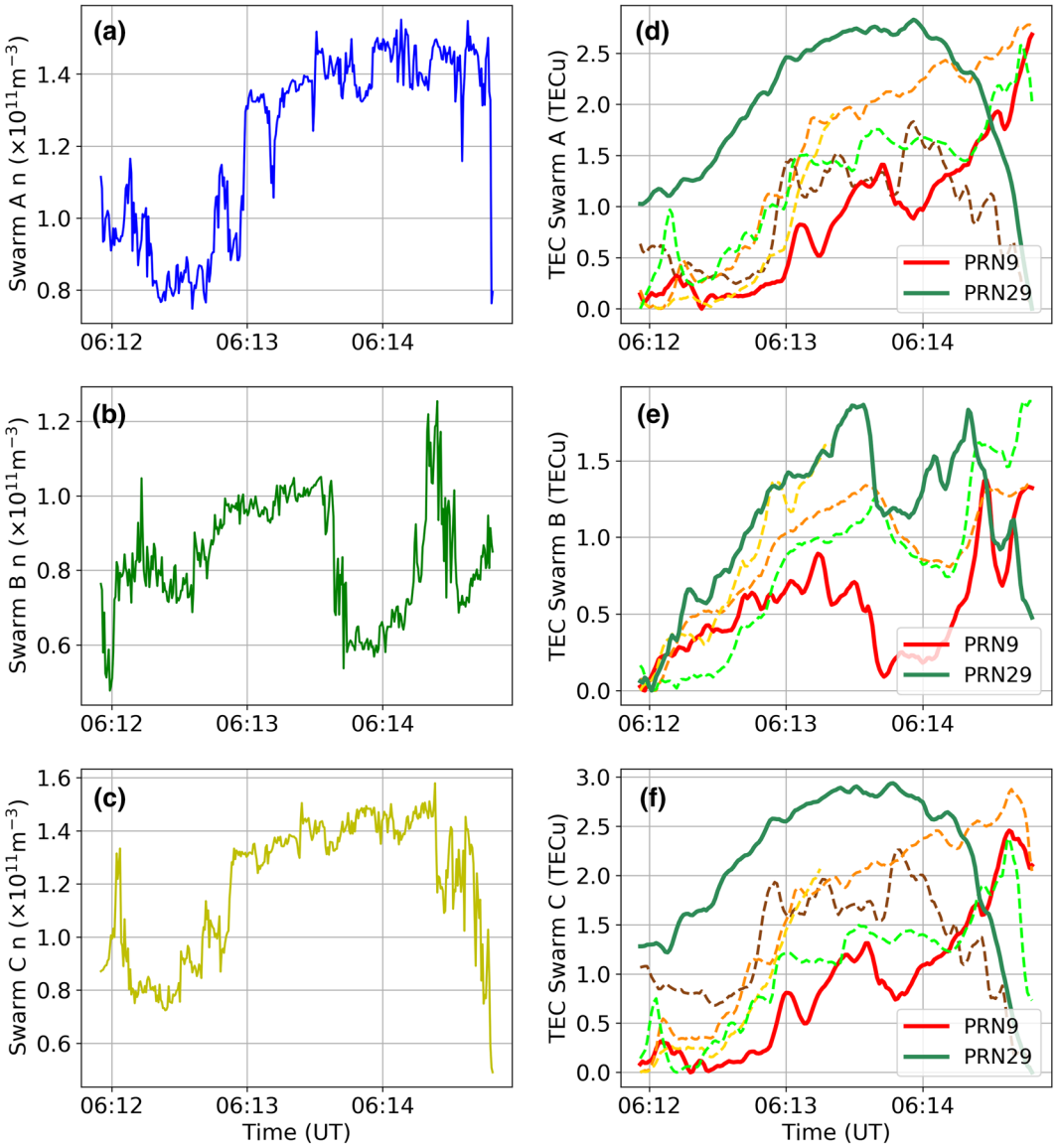

Figure 5. Results from 1 November 2015, 06:11:55 to 06:14:49 UT. The format is the same as in Figure 3.

which Swarm A enters around 22:58:30 UT, but the coverage is too limited to provide more detailed information about the spatial extent of the density enhancement. We therefore conclude that ground-based observations provide some support our findings, although they cannot confidently confirm them.

4.4.2. Case 2: 1 November 2015

Case 2 is from 1 November 2015, around 6:12 a.m. UT. Data from the Swarm instruments are shown in Figure 5, in the same format as Figure 3.

We observe in panels (a) and (c) that Swarm A and C move from a low-density area of $n \approx 1 \times 10^{11}$ m^{-3} into a higher-density area of $n \approx 1.45 \times 10^{11}$ m^{-3} around 06:13 UT. Swarm B Langmuir probe measurements shown in panel (b) fluctuate between 0.5 and 1.2 $\times 10^{11}$ m^{-3}, with a plateau centered around 06:13 UT and a large spike at 06:14:30 UT.

Panels (d)–(f) show the TEC variations from Swarm A, B, and C, respectively. As before, we remove background TEC for each PRN separately, and we have highlighted two GPS satellites (PRN9 and PRN29) that we will consider in more detail. Swarm A/C tracks PRN9 at a 225° angle (port side/aft) and 45° elevation. TEC estimates from Swarm A/C to PRN9 show a steady increase throughout the event, with a start value of 0 TECu and end value of 2.5 TECu. These TEC observations imply a density enhancement toward the end

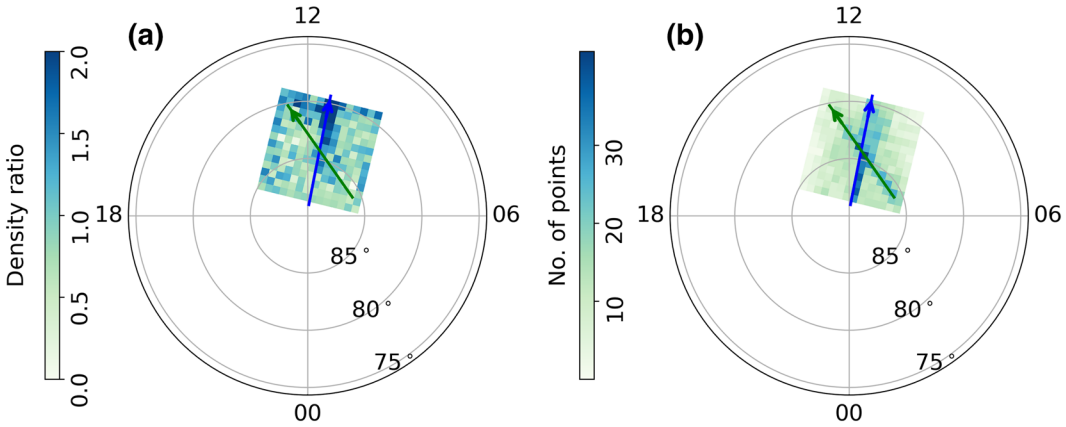

Figure 6. Results from 1 November 2015, 06:11:55 to 06:14:49 UT. The format is the same as in Figure 4.

of the event for Swarm A/C, localized to the port side of their trajectories. Swarm B tracks PRN9 at a 265° azimuth (port side), and its TEC measurements show a small increase around 06:13 UT, before a small dip around 06:14. Toward the end of the event, TEC rises again to 1.4 TECu.

TEC calculations from GPS satellite PRN29 are shown in dark green color in panels D-F of Figure 5. The GPS satellite is tracked by Swarm A/C at a 45° (starboard/forward) and 34° elevation. In panels (d) and (f), we see that TEC is 1–1.3 TECu, before it slowly increases to 2.8 TECu at 06:14 UT. Toward the end of the event, TEC drops sharply and ends at 0 TECu. Thus, we expect a density enhancement to occur around 06:13–06:14 UT, and somewhat to the starboard side, although the elevation of PRN29 is high; thus, the spatial extent will not be large. Swarm B tracks PRN29 at an almost 90° angle, that is, on the starboard side. For Swarm B, PRN29 TEC estimates are lower, starting at 0 TECu at the beginning of the event, and peaking at 1.8 TECu at 06:13 UT.

Results from the reconstruction are shown in Figure 6, in the same format as Figure 4. The inversion result suggests a significant density enhancement where the density ratio is about 1.5–2. It is centered on 11.5 MLT, 80° MLAT and confined to the vicinity of the orbit, with a small longitudinal and somewhat larger latitudinal extent.

Panel (b) shows the number of non-zero entries in **F** matrix, that is, how many times that grid cell has contribution to a TEC time series. This event shows a very high concentration of data points close to the Swarm trajectories, indicating that the elevations of tracked GPS satellites are high. Another contributing factor is the calculated plasma temperature, which is relatively high ($T_i \approx 3200$ K) compared to other events studied.

4.4.3. Comparison With Ground-Based GPS TEC

We compare the inversion results for Case 2 with ground-based observations of TEC obtained through the Madrigal database, shown in Figure 7, with the trajectories of Swarm A and B as well as the grid overlaid. Again, the coordinate system is MLT-MLAT. We have included data from a ten minute interval and smoothed the data using median filtering (see section 2) to compensate for the limited data availability. Panel (a) shows the observed TEC, while in panel (b) the TEC is divided by the average TEC in the polar cap (MLAT > 80°) to show the density distribution in a similar manner to Figure 6. Like the estimated density variations calculated with the inversion procedure, Figure 7 shows a TEC enhancement centered on 11.5 MLT, 80° MLAT. The density in the patch is approximately 8–9 TECu, while the background density is around 3–4 TECu. The relative increase compared to the background is also of similar magnitude to that shown in the reconstruction. In the ground-based observations, the enhancement has a larger extent in longitude and latitude than the reconstruction, which may reflect the vertical structure of the plasma density enhancement. If we run the reconstruction procedure with an imposed plasma temperature of 1000 K, the results show a density distribution (not shown) that agrees better with the ground-based observations. The inversion result with a plasma of temperature 1000 K shows a density enhancement with larger extent than what is shown in Figure 6, although it is still smaller in size than the ground-based observations.

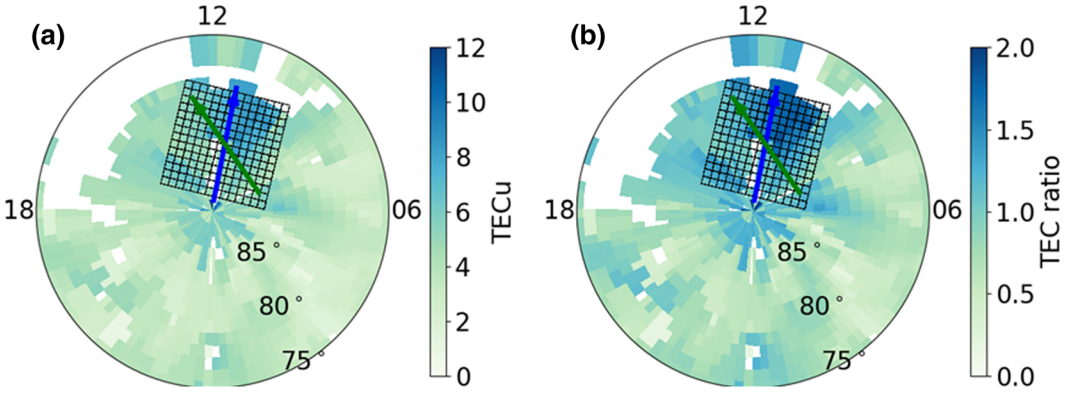

Figure 7. Ground-based GPS TEC observations from 1 November 2015, 06:07–06:17 UT. The data have been median filtered (see text for details). (a) Absolute TEC. (b) TEC divided by average TEC in the polar cap (MLAT > 80°). Notice the different color scales.

5. Discussion

This paper has presented a new method that utilizes Swarm's three-satellite configuration to deduct information about the density distribution in the plane surrounding the satellites. We have presented a synthetic data case to demonstrate the concept, including weight factors to account for scale height and discretization issues. Through sensitivity studies we find optimal input parameters for the synthetic test case, which yield satisfactory results with a RMS error of 0.263 between the given input density distribution and the reconstruction. As concluded in the sensitivity analysis, we apply a 10 s step length and use all three Swarm satellites when we apply the inversion method to real-world cases. Results show that Langmuir probe density measurements and TEC estimates from Swarm GPS receivers (e.g., Figures 3 and 5) are in agreement with our reconstructed plasma density (e.g., Figures 4 and 6). The availability of ground-based GPS TEC data for verification is limited in the polar cap due to the sparse number of receivers. However, for one of our real-world cases, there is sufficient ground-based GPS TEC coverage to conclude that ground-based observations confirm our method (Figure 7). The lack of coverage of ground-based observations in the polar cap only proves that our new method fills a knowledge cap in the area of nowcasting the ionosphere's electron content.

The density reconstruction technique ultimately condenses the ionosphere into a thin shell. Vertical density variations are considered in the weight matrix **F** in the sense that contributions to the density on the grid correspond to the altitude of the Swarm satellite in consideration. The choice of LEO satellites, or more specifically, the LEO satellites' orbit altitude, to use in the technique is therefore important.

The Swarm satellites orbit at 462/511 km altitude, which is above the peak plasma density region usually found around 250 km altitude (Kelley, 2009). Furthermore, Lorentzen et al. (2004) used observations from two all-sky imagers on Svalbard, Norway, and applied triangulation technique to calculate the altitude of two patches, which was found to be located at altitudes of 310 (±25) and 320 (±25) km, which is consistent with earlier findings (Rodger et al., 1994). The Swarm satellites at orbiting at 462/511 km altitude are thus approximately 3–3.5 times the scale height above the peak patch density. Nevertheless, the density variations will map along the magnetic field lines due to the frozen in condition (Kelley, 2009), such that they are captured by Swarm instruments at the higher altitudes. We therefore argue that even though the Swarm satellites are in all likelihood always located above the peak plasma density altitude, the reconstruction algorithm can accurately capture the salient density variations in the polar cap, due to the frozen in condition.

Our results show that the reconstruction method is crude, and generally tends to perform better when the density variations are significant, which echoes our previous discussion on the discrepancy between plasma and polar cap patch peak altitude and Swarm satellite orbit altitude. Examining the total data set of 520 events spread over the course of 2014–2018, we noticed that the quality of results declined in the latter years. This decline is likely related to the solar cycle, which had a peak in 2013 and a minimum around 2018-2019. It is known that when solar activity is low, TEC in the polar cap is correspondingly low (Jin et al., 2019). Since the inversion technique is rather crude, we are not able to capture the subtle density variations that occur when solar activity is low.

We have also seen that the satellite constellation geometry is important for the accuracy of the results. Expanding the technique to a larger constellation of LEO satellites will increase both coverage area and accuracy of results, as confirmed by our sensitivity study. Due to the characteristics of Swarm satellite trajectory evolution, we have so far only been able to analyze cases where the separation between Swarm A/C and B is up to about 3 hr MLT. In the coming years, the separation between the lower pair and the upper satellite will increase. In 2021, Swarm B's orbit will be anti parallel to A/C. This geometry could be interesting to consider for the inversion technique.

Our inversion method is applicable to lower latitudes as well, with some modifications. The separation between the A-C pair and B is too large to use all three satellites, but we can make the inversion with TEC data from only A and C, although we expect somewhat less accurate results, as indicated by the sensitivity analysis. Furthermore, since A and C are nearly parallel, we have less information about the spatial extent of density variations than we do in the polar caps. However, we have seen examples (one is attached in supporting information Figure S15) were the inversion procedure shows promising results at equatorial latitudes.

The inversion technique demonstrated in this paper does not attempt to reproduce the absolute density values in the ionosphere. As previously discussed, the altitude of the Swarm satellites is above the ionospheric density peak layer. Furthermore, as mentioned previously, the TEC value computed by the GPS receiver includes the plasmaspheric section of the GPS ray path. Although we avoid the main plasmaspheric contribution to TEC by removing bias from the time series, we cannot expect to accurately reproduce absolute densities. However, in relation to space weather forecasting in the polar regions, information about absolute density values is not vital. It is known that it is the large density gradients associated with polar cap patches that result in the most severe scintillations on GPS signals (e.g., Buchau et al., 1985; Basu et al., 2002; Clausen et al., 2016; Jin, Moen, et al., 2014; Jin et al., 2016; Meeren et al., 2015; Prikryl et al., 2010; Spogli et al., 2009; Weber et al., 1986).

Our technique presents a novel contribution to space weather forecasting in the sense that we estimate density variations in the horizontal (i.e. ultimately spherical) plane and that we do not rely on ground-based receivers. The method is unique in that it takes advantage of the multisatellite constellation to provide information about the spatial extent of polar cap patches. It is relevant to nowcasting the state of the ionosphere and, in particular, the prediction of polar cap patches. The presented method used the Langmuir Probe for two of the weight factors, but there is an opportunity to assume a temperature and density difference based on scale height, thus enabling the use of the method to rely on GPS receiver data only. The method could be expanded to include more LEO satellites with dual-frequency GPS receivers on board, ultimately providing continuous coverage of the ionosphere, including low latitudes. This abundance of data would release a vast amount of information on density variations, which is valuable for further study of dynamic phenomena in the ionosphere, such as polar cap patches and density gradients. The satellite based reconstruction technique enables observation of the ionosphere in regions where we have little or no ground-based observations, for example, Antarctica and the oceans.

Some questions remain unanswered and must be addressed in further development of this method. The sensitivity analyses, as well as the real cases, showed that the algorithm is sensitive to the plasma temperature. As previously mentioned, Case Study 2 (1 November 2015) is an example (out of several events) that showed better agreement with ground-based TEC estimates for an imposed plasma temperature that was lower than the calculated temperature based on the ratio of Langmuir probe density estimates from two satellites. Confirming the plasma temperature using Swarm's Thermal Ion Imager (Knudsen et al., 2017), would further consolidate our findings.

6. Conclusion

This paper has presented a novel method to calculate two-dimensional density variations in the polar cap, using the three-satellite Swarm constellation and their GPS receivers. Additionally, we use Langmuir probe data for weighting factors that improve the accuracy of the inversion. We have demonstrated the usefulness of the method using a test case with synthetic data as well as real-world cases, which are confirmed by Langmuir probe density estimates and ground-based GPS TEC data. Sensitivity analyses on the synthetic data provide the optimal input parameters for the model. The reconstruction method was shown to be sensitive

to satellite configuration geometry and plasma temperature, and it captures large density variations well. In the future, including more LEO satellites will increase the number of data points and thus the quality of the results. The GPS TEC based reconstruction technique is important due to its relevance to space weather forecasting, and in particular, detection and prediction of polar cap patches. Monitoring the ionosphere without depending on ground stations is a significant step forward toward space weather forecasting.

Data Availability Statement

Swarm data products are available through the official Swarm data access platform (https://swarm-diss.eo.esa.int/). GPS TEC data products and access through the Madrigal distributed data system are provided to the community (http://www.openmadrigal.org) by the Massachusetts Institute of Technology (MIT) under support from U.S. National Science Foundation Grant AGS-1242204. Data for TEC processing is provided from the following organizations: UNAVCO, Scripps Orbit and Permanent Array Center, Institut Geographique National, France, International GNSS Service, The Crustal Dynamics Data Information System (CDDIS), National Geodetic Survey, Instituto Brasileiro de Geografia e Estatística, RAMSAC CORS of Instituto Geográfico Nacional de la República Argentina, Arecibo Observatory, Low-Latitude Ionospheric Sensor Network (LISN), Topcon Positioning Systems, Inc., Canadian High Arctic Ionospheric Network, Centro di Ricerche Sismologiche, Systéme d'Observation du Niveau des Eaux Littorales (SONEL), RENAG: REseau NAtional GPS permanent, GeoNet (the official source of geological hazard information for New Zealand), GNSS Reference Networks, Finnish Meteorological Institute, and SWEPOS-Sweden. Access to these data is provided by madrigal network via https://cedar.openmadrigal.org/ website.

Acknowledgments
This work received financial support from the European Space Agency (Contract 4000114121/15/NL/MP) in the framework of the STSE (Support To Science Element) Swarm+Innovation Program. Swarm is a European Space Agency mission with major support from the Canadian Space Agency for the EFI. Swarm data can be accessed from ESA's data access Web page (https://earth.esa.int/web/guest/swarm/data-access). This research is a part of the 4DSpace Strategic Research Initiative at the University of Oslo.

References

Aarons, J. (1982). Global morphology of ionospheric scintillations. *Proceedings of the IEEE*, *70*(4), 360–378. https://doi.org/10.1109/PROC.1982.12313

Alfonsi, L., Spogli, L., De Franceschi, G., Romano, V., Aquino, M., Dodson, A., & Mitchell, C. N. (2011). Bipolar climatology of GPS ionospheric scintillation at solar minimum. *Radio Science*, *46*, RS0D05. https://doi.org/10.1029/2010RS004571

Basu, S., Groves, K. M., Basu, S., & Sultan, P. J. (2002). Specification and forecasting of scintillations in communication/navigation links: Current status and future plans. *Journal of Atmospheric and Solar-Terrestrial Physics*, *64*(16), 1745–1754. https://doi.org/10.1016/S1364-6826(02)00124-4

Buchau, J., Weber, E. J., Anderson, D. N., Carlson Jr., H. C., Moore, J. G., Reinisch, B. W., & Livingston, R. C. (1985). Ionospheric structures in the polar cap: Their origin and relation to 250-MHz scintillation, *20*(3), 325–338. https://doi.org/10.1029/RS020i003p00325

Bust, G. S., Crowley, G., Garner, T. W., Gaussiran II, T. L., Meggs, R. W., Mitchell, C. N., et al. (2007). Four-dimensional GPS imaging of space weather storms. *Space Weather*, *5*, S02003. https://doi.org/10.1029/2006SW00237

Bust, G. S., Garner, T. W., & Gaussiran II, T. L. (2004). Ionospheric Data Assimilation Three-Dimensional (IDA3D): A global, multisensor, electron density specification algorithm. *Journal of Geophysical Research*, *109*, A11312. https://doi.org/10.1029/2003JA010234

Chen, C. H., Saito, A., Lin, C. H., Yamamoto, M., Suzuki, S., & Seemala, G. K. (2016). Medium-scale traveling ionospheric disturbances by three-dimensional ionospheric GPS tomography. *Earth, Planets and Space*, *68*(1), 32. https://doi.org/10.1186/s40623-016-0412-6

Clausen, L. B. N., Moen, J. I., Hosokawa, K., & Holmes, J. M. (2016). GPS scintillations in the high latitudes during periods of dayside and nightside reconnection. *Journal of Geophysical Research: Space Physics*, *121*, 3293–3309. https://doi.org/10.1002/2015JA022199

Coley, W. R., & Heelis, R. A. (1995). Adaptive identification and characterization of polar ionization patches. *Journal of Geophysical Research*, *100*(A12), 23,819–23,827. https://doi.org/10.1029/95JA02700

Crowley, G. (1996). Critical review of ionospheric patches and blobs. In W. R. Stone (Ed.), *Review of radio science 1993–1996* (pp. 619–648). United Kingdom: Oxford Science Publication.

De Franceschi, G., Alfonsi, L., Romano, V., Aquino, M., Dodson, A., Mitchell, C. N., et al. (2008). Dynamics of high-latitude patches and associated small-scale irregularities during the October and November 2003 storms. *Journal of Atmospheric and Solar-Terrestrial Physics*, *70*(6), 879–888. https://doi.org/10.1016/j.jastp.2007.05.018

Dos Santos Prol, F., de Oliveira Camargo, P., Hernndez-Pajares, M., & de Assis Honorato Muella, M. T. (2019). A new method for ionospheric tomography and its assessment by ionosonde electron density, GPS TEC, and single-frequency PPP. *IEEE Transactions on Geoscience and Remote Sensing*, *57*(5), 2571–2582. https://doi.org/10.1109/TGRS.2018.2874974

Friis-Christensen, E., Lhr, H., & Hulot, G. (2006). Swarm: A constellation to study the Earth's magnetic field. *Earth, Planets and Space*, *58*(4), 351–358. https://doi.org/10.1186/bf03351933

Garner, T. W., Harris, R. B., York, J. A., Herbster, C. S., Minter III, C. F., & Hampton, D. L. (2011). An auroral scintillation observation using precise, collocated GPS receivers. *Radio Science*, *46*, RS1018. https://doi.org/10.1029/2010rs004412

Goodwin, L. V., Iserhienrhien, B., Miles, D. M., Patra, S., van der Meeren, C., Buchert, S. C., et al. (2015). Swarm in situ observations of f region polar cap patches created by cusp precipitation. *Geophysical Research Letters*, *42*, 996–1003. https://doi.org/10.1002/2014GL062610

Hosokawa, K., Shiokawa, K., Otsuka, Y., Nakajima, A., Ogawa, T., & Kelly, J. D. (2006). Estimating drift velocity of polar cap patches with all-sky airglow imager at Resolute Bay, Canada. *Geophysical Research Letters*, *33*, L15111. https://doi.org/10.1029/2006GL026916

Jacobsen, K. S., & Andalsvik, Y. L. J. J. S. W. S. C. (2016). Overview of the 2015 St. Patrick's Day storm and its consequences for RTK and PPP positioning in Norway, *6*, A9.

Jin, S., Cardellach, E., & Xie, F. (2014). *Gnss remote sensing—Theory, methods and applications*. Dordrect, Netherlands: Springer.

Jin, Y., Moen, J. I., & Miloch, W. J. (2014). Gps scintillation effects associated with polar cap patches and substorm auroral activity: Direct comparison. *Journal Space Weather Space Climate*, *4*, A23.

Jin, Y., Moen, J. I., & Miloch, W. J. (2015). On the collocation of the cusp aurora and the GPS phase scintillation: A statistical study. *Journal of Geophysical Research: Space Physics*, *120*, 9176–9191. https://doi.org/10.1002/2015ja021449

Jin, Y., Moen, J. I., Miloch, W. J., Clausen, LasseB. N., & Oksavik, K. (2016). Statistical study of the GNSS phase scintillation associated with two types of auroral blobs. *Journal of Geophysical Research: Space Physics*, *121*, 4679–4697. https://doi.org/10.1002/2016JA022613

Jin, Y., & Oksavik, K. (2018). GPS scintillations and losses of signal lock at high latitudes during the 2015 St. Patrick's Day storm, *123*(9), 7943–7957. https://doi.org/10.1029/2018JA025933

Jin, Y., Spicher, A., Xiong, C., Clausen, . B. N., Kervalishvili, G., Stolle, C., & Miloch, W. J. (2019). Ionospheric plasma irregularities characterized by the Swarm satellites: Statistics at high latitudes. *Journal of Geophysical Research: Space Physics*, *124*, 1262–1282. https://doi.org/10.1029/2018JA026063

Kelley, M. C. (2009). *The Earth's ionosphere: Plasma physics and electrodynamics* (Vol. 96). London, England: Academic Press.

Kintner, P. M., Ledvina, B. M., & Paula, E. R. (2007). GPS and ionospheric scintillations. *Space Weather*, *5*, S09003. https://doi.org/10.1029/2006sw000260

Knudsen, D. J., Burchill, J. K., Buchert, S. C., Eriksson, A. I., Gill, R., Wahlund, J.-E., et al. (2017). Thermal ion imagers and Langmuir probes in the Swarm electric field instruments. *Journal of Geophysical Research: Space Physics*, *122*, 2655–2673. https://doi.org/10.1002/2016ja022571

Leitinger, R., Ladreiter, H.-P., & Kirchengast, G. (1997). Ionosphere tomography with data from satellite reception of global navigation satellite system signals and ground reception of navy navigation satellite system signals. *Radio Science*, *32*(4), 1657–1669. https://doi.org/10.1029/97RS01027

Li, H., Yuan, Y., Li, Z., Huo, X., & Yan, W. (2012). Ionospheric electron concentration imaging using combination of leo satellite data with ground-based GPS observations over China. *IEEE Transactions on Geoscience and Remote Sensing*, *50*(5), 1728–1735. https://doi.org/10.1109/TGRS.2011.2168964

Lorentzen, D. A., Shumilov, N., & Moen, J. (2004). Drifting airglow patches in relation to tail reconnection. *Geophysical Research Letters*, *31*, L02806. https://doi.org/10.1029/2003GL017785

Ma, X. F., Maruyama, T., Ma, G., & Takeda, T. (2005). Three-dimensional ionospheric tomography using observation data of GPS ground receivers and ionosonde by neural network. *Journal of Geophysical Research*, *110*, A05308. https://doi.org/10.1029/2004JA010797

Meeren, C., Oksavik, K., Lorentzen, D. A., Rietveld, M. T., & Clausen, L. B. N. (2015). Severe and localized GNSS scintillation at the poleward edge of the nightside auroral oval during intense substorm aurora. *Journal of Geophysical Research: Space Physics*, *120*, 10,607–10,621. https://doi.org/10.1002/2015JA021819

Mitchell, C. N., Alfonsi, L., De Franceschi, G., Lester, M., Romano, V., & Wernik, A. W. (2005). Gps tec and scintillation measurements from the polar ionosphere during the October 2003 storm. *Geophysical Research Letters*, *32*, L12S03. https://doi.org/10.1029/2004gl021644

Moen, J., Oksavik, K., Alfonsi, L., Daabakk, Y., Romano, V., & Spogli, L. (2013). Space weather challenges of the polar cap ionosphere. *Journal Space Weather Space Climate*, *3*, A02. https://doi.org/10.1051/swsc/2013025

Noja, M., Stolle, C., Park, J., & Lhr, H. (2013). Long-term analysis of ionospheric polar patches based on Champ TEC data. *Radio Science*, *48*, 289–301. https://doi.org/10.1002/rds.20033

Olsen, N., Friis-Christensen, E., Floberghagen, R., Alken, P., Beggan, C. D., Chulliat, A., et al. (2013). The Swarm Satellite Constellation Application and Research Facility (SCARF) and Swarm data products. *Earth, Planets and Space*, *65*(11), 1.

Prikryl, P., Jayachandran, P. T., Chadwick, R., & Kelly, T. D. (2015). Climatology of GPS phase scintillation at northern high latitudes for the period from 2008 to 2013. *Annales Geophysicae*, *33*, 531–545. https://doi.org/10.5194/angeo-33-531-2015

Prikryl, P., Jayachandran, P. T., Mushini, S. C., Pokhotelov, D., MacDougall, J. W., Donovan, E., et al. (2010). GPS TEC, scintillation and cycle slips observed at high latitudes during solar minimum. *Annales Geophysicae*, *28*, 1307–1316. https://doi.org/10.5194/angeo-28-1307-2010

Pryse, S., & Kersley, L. (1992). A preliminary experimental test of ionospheric tomography. *Journal of Atmospheric and Terrestrial Physics*, *54*(7-8), 1007–1012.

Pryse, S. E., Kersley, L., Mitchell, C. N., Spencer, P. S. J., & Williams, M. J. (1998). A comparison of reconstruction techniques used in ionospheric tomography. *Radio Science*, *33*(6), 1767–1779. https://doi.org/10.1029/98RS01613

Raymund, T. (1995). Comparison of several ionospheric tomography algorithms. *Annales Geophysicae*, *13*(13), 1254–1262.

Raymund, T. D., Austen, J. R., Franke, S. J., Liu, C. H., Klobuchar, J. A., & Stalker, J. (1990). Application of computerized tomography to the investigation of ionospheric structures. *Radio Science*, *25*(5), 771–789. https://doi.org/10.1029/RS025i005p00771

Raymund, T. D., Pryse, S. E., Kersley, L., & Heaton, J. A. T. (1993). Tomographic reconstruction of ionospheric electron density with European incoherent scatter radar verification. *Radio Science*, *28*(5), 811–817. https://doi.org/10.1029/93RS01102

Rideout, W., & Coster, A. (2006). Automated GPS processing for global total electron content data. *GPS Solutions*, *10*(3), 219–228. https://doi.org/10.1007/s10291-006-0029-5

Rodger, A. S., Pinnock, M., Dudeney, J. R., Baker, K. B., & Greenwald, R. A. (1994). A new mechanism for polar patch formation. *Journal of Geophysical Research*, *99*(A4), 6425–6436. https://doi.org/10.1029/93JA01501

Snyman, J. A. (2005). *Practical mathematical optimization*. Cham, Switzerland: Springer.

Spencer, P., Kersley, L., & Pryse, S. E. (1998). A new solution to the problem of ionospheric tomography using quadratic programming. *Radio Science*, *33*(3), 607–616. https://doi.org/10.1029/98RS00694

Spicher, A., Clausen, L. B. N., Miloch, W. J., Lofstad, V., Jin, Y., & Moen, J. I. (2017). Interhemispheric study of polar cap patch occurrence based on Swarm in situ data. *Journal of Geophysical Research: Space Physics*, *122*, 3837–3851. https://doi.org/10.1002/2016JA023750

Spogli, L., Alfonsi, L., De Franceschi, G., Romano, V., Aquino, M. H. O., & Dodson, A. (2009). Climatology of GPS ionospheric scintillations over high and mid-latitude European regions. *Annales Geophysicae*, *27*(9), 3429–3437. https://doi.org/10.5194/angeo-27-3429-2009

Thomas, E. G., Baker, J. B. H., Ruohoniemi, J. M., Clausen, L. B. N., Coster, A. J., Foster, J. C., & Erickson, P. J. (2013). Direct observations of the role of convection electric field in the formation of a polar tongue of ionization from storm enhanced density. *Journal of Geophysical Research: Space Physics*, *118*, 1180–1189. https://doi.org/10.1002/jgra.50116

Tsai, L.-C., Liu, C., Tsai, W., & Liu, C. (2002). Tomographic imaging of the ionosphere using the GPS/MET and NNSS data. *Journal of Atmospheric and Solar-Terrestrial Physics*, *64*(18), 2003–2011.

van den IJssel, J., Forte, B., & Montenbruck, O. (2016). Impact of Swarm GPS receiver updates on pod performance. *Earth, Planets and Space*, *68*(1), 85.

van den Ijssel, J., Encarnacao, J., Doornbos, E., & Visser, P. (2015). Precise science orbits for the Swarm satellite constellation. *Advances in Space Research*, *56*(6), 1042–1055. https://doi.org/10.1016/j.asr.2015.06.002

Vierinen, J., Coster, A. J., Rideout, W. C., Erickson, P. J., & Norberg, J. (2016). Statistical framework for estimating GNSS bias. *Atmospheric Measurement Techniques*, *9*(3), 1303–1312. https://doi.org/10.5194/amt-9-1303-2016

Weber, E. J., Buchau, J., Moore, J. G., Sharber, J. R., Livingston, R. C., Winningham, J. D., & Reinisch, B. W. (1984). *F* layer ionization patches in the polar cap. *Journal of Geophysical Research*, *89*(A3), 1683–1694. https://doi.org/10.1029/JA089iA03p01683

Weber, E. J., Klobuchar, J. A., Buchau, J., Carlson, H. C., Livingston, R. C., de la Beaujardiere, O., et al. (1986). Polar cap f layer patches: Structure and dynamics. *Journal of Geophysical Research*, *91*(A11), 12,121–12,129. https://doi.org/10.1029/JA091iA11p12121

Yeh, K. C., & Liu, C.-H. (1982). Radio wave scintillations in the ionosphere. *Proceedings of the IEEE*, *70*(4), 324–360. https://doi.org/10.1109/PROC.1982.12313

Zhou, C., Lei, Y., Li, B., An, J., Zhu, P., Jiang, C., et al. (2015). Comparisons of ionospheric electron density distributions reconstructed by GPS computerized tomography, backscatter ionograms, and vertical ionograms. *Journal of Geophysical Research: Space Physics*, *120*, 11,032–11,047. https://doi.org/10.1002/2015JA021855